PORE-SCALE MODELLING: EFFECTS OF NETWORK PROPERTIES ON PREDICTIVE CAPABILITIES

Nasiru Idowu, Cyril Nardi, Haili Long and Pål-Eric Øren
Numerical Rocks AS, Stiklestadveien 1, 7041 Trondheim, Norway

This paper was prepared for presentation at the International Symposium of the Society of Core Analysts held in Aberdeen, Scotland, UK, 27-30 August, 2012

ABSTRACT

We examine three different methods of extracting skeletons from micro-CT (MCT) images of rock samples. Two of the methods are pore-based: thinning algorithm and distance-ordered homotopic thinning while the third one is a grain-based algorithm. Skeletons are extracted from MCT images of Berea, Bentheimer and Fontainebleau. Using the same geometrical characterization and partitioning, pore networks are then generated from these skeletons. Multiphase displacements are simulated on the pore networks and results such as network properties, single and multiphase transport properties are compared to assess the impacts of the different methods on both pore network properties and simulated results. The results are also compared with those computed directly on the MCT images.

Comparison of the different networks from each image shows differences in the pore-networks parameters such as number of pores and average connectivities (coordination number). The predicted single-phase transport properties obtained from networks generated from two of the skeletonization methods are comparable with grid-predicted data. However, the predicted primary drainage relative permeability and capillary pressure curves, initial water saturation, imbibition relative permeability curves and residual oil saturation for the different networks from all the three skeletonization methods for each sample are similar under strongly water-wet conditions.

There are also good agreements between the network-predicted relative permeability curves, grid-predicted relative permeability curves and available experimental data for both Berea and Bentheimer images. Multiphase simulations at mixed-wet and oil-wet conditions are performed on the different Fontainebleau networks and the imbibition relative permeability curves are also similar under both wetting conditions. We therefore conclude that even though pore network extraction is a non-unique process, predicted multi-phase transport properties are consistent if the topology of the pore space is well preserved in the extracted skeleton.

INTRODUCTION

Interest in the use of digital rock technology (pore-scale imaging and modelling) is growing considerably. This trend is facilitated by the continual improvement being made in the representation of rock samples through direct 3D imaging of the pore space and our improved understanding of the pore-scale displacement physics. It is now possible to simulate multiphase flow directly on digitised images and predict multiphase transport properties that are in good agreement with experimental data, using two-phase Lattice Boltzmann simulations (Ramstad *et al.* [1]). However, these simulations are computationally expensive and are also resolution dependent.

Pore network models offer an alternative approach with good computational speed and infinite resolutions to direct simulations on grids. These models however, require simplified but representative networks of pores and throats extracted from digitised images of rock samples. A number of algorithms exists to extract topologically equivalent skeletons from voxelized images and the extracted networks of pores and throats can then be characterized geometrically.

Algorithms for extracting skeleton from 3D images can be broadly categorized into two: pore-based and grain-based algorithms. Medial axis is a pore-based approach which could be based on either thinning algorithms [2-4] or on burning algorithms, Lindquist *et al.* [5]. Thinning algorithms are procedures for iteratively deleting of individual voxels while preserving topological properties. We used an open-source pore-based thinning algorithm (PBTA) image processing software called ImageJ/Fiji and distance ordered homotopic thinning (DOHT) algorithm in a commercial software called Avizo.

The inverse function of thinning is dilation and the grain-based algorithm used is based on ultimate dilation of the grain network, Bakke and Øren [6]. The skeleton of the pore network is found where two or more dilated grain border surface meet. This line is defined by the points in space which have neighbour voxels from 3 or more different dilated grains. We used in-house grain-based algorithm (GBA) in our proprietary e-Core software. Previous studies carried out to assess the impact of different skeletonization algorithms, Dong *et al.* [7] or sensitivity of numerical simulations to differences in network topology, Bhattad *et al.* [8] neither compared the predicted results with experimental data nor assessed the accuracy of predicted transport properties.

In this study, we evaluate the impacts of three different methods of extracting skeletons from MCT images and pore networks generated thereafter on both pore network properties and simulated results. Predicted single-phase transport properties, primary drainage capillary pressure and relative permeability curves, and imbibition relative permeability curves for the different networks are compared for each sample. The results are also compared with available experimental data and direct simulations on the grids. We briefly describe the samples, present results and then provide some explanations to the differences observed in the network properties and the consistency in the multiphase transport properties in the following sections.

DESCRIPTION OF SAMPLES AND EXTRACTED PORE NETWORKS

Table 1 summarises the petrophysical data obtained by applying a Lattice-Boltzmann (LBM) simulation [9] directly on the Berea, Bentheimer and Fontainebleau digitised sandstone images. In our study we used outcrops that are well-sorted, homogeneous and consist mainly of quartz and feldspar with little amount of clay or no clay at all. These samples have comparable petrophysical properties (absolute permeabilities) as the experimental rocks allowing us to compare both sets of results directly. Three different skeletons were extracted for each sample using the GBA, PBTA and DOHT algorithms described above. Using the same geometrical characterization and partitioning, pore networks are then generated from these skeletons. The three different networks generated for Berea_01 sample are shown in Figure 1.

Table 1. Petrophysical properties of the samples computed on the grids. Permeability values are obtained from LBM simulations

	Size (voxels)	Resolution (μm)	Clay Content (%)	Permeability (mD)	Porosity (%)
Berea_01	400×400×400	5.35	0	1,345	19.65
Berea_02	900×900×900	1.50	3.58	409	16.97
Bentheimer	400×400×400	6.70	1.10	1,949	20.55
Fontainebleau	480×480×480	5.70	0	2,551	21.00

The number of pores and the average connectivities of the networks generated from the different skeletons are summarised in Table 2, and pore and throat radius distributions are shown in Figure 2.

Table 2. Number of pores generated from skeletons extracted from GBA, PBTA and DOHT algorithms. The average connectivities are in brackets.

	Berea_01	Berea_02	Bentheimer	Fontainebleau
GBA	7,811	17,024	8,978	11,747
	(4.27)	(5.81)	(4.30)	(4.58)
PBTA	12,725	38,854	13,958	12,596
	(3,35)	(3.66)	(3.49)	(3.48)
DOHT	13,138	37,615	13,933	12,814
	(3.33)	(3.59)	(3.39)	(3.48)

RESULTS

Pore Network Properties

The general trend observed in Table 2 is that networks extracted from PBTA and DOHT skeletons have similar and comparable number of pores because both methods are based on thinning algorithm while GBA have lower number of pores. However, the average connectivities of networks from GBA are greater than those from the other two methods. The pore and throat radius distributions of networks generated from both PBTA and

DOHT skeletons are also similar as depicted in Figure 2 while those from GBA show larger pores and throats.

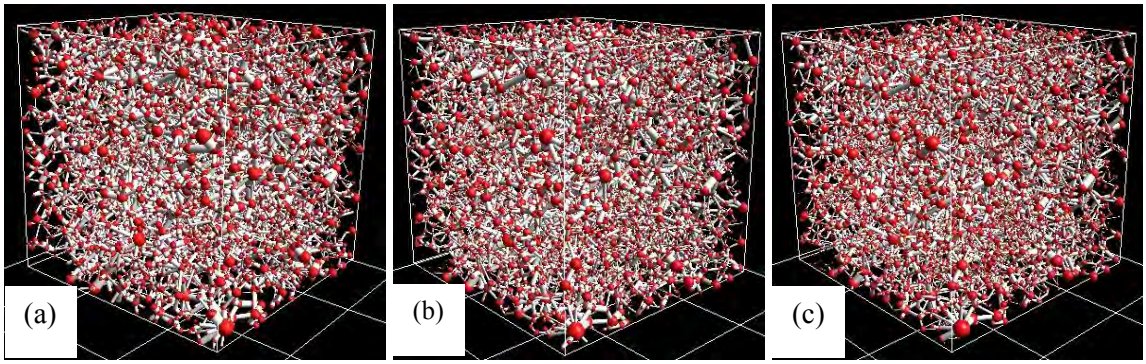

Figure 1: Pore networks for Berea_01 sample from (a) GBA, (b) PBTA, and (c) DOHT skeletons

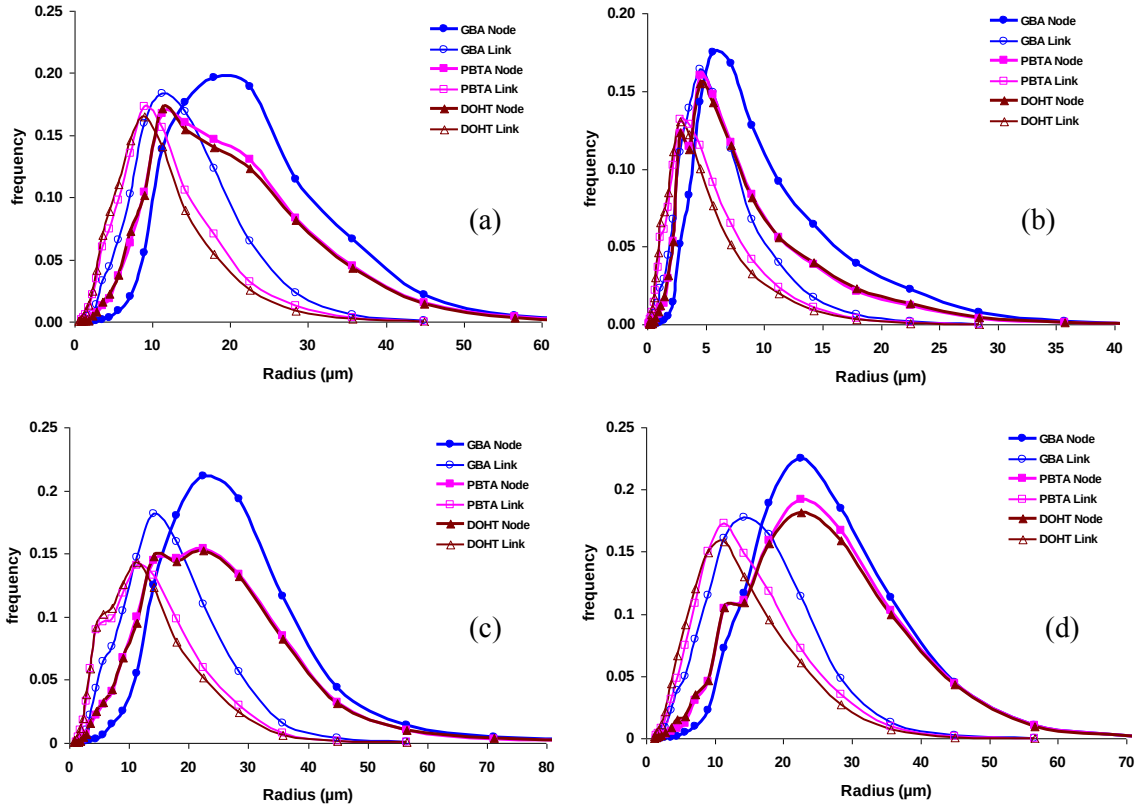

Figure 2: Pore (node) and throat (link) radius distributions for (a) Berea_01, (b) Berea_02, (c) Bentheimer and (d) Fontainebleau networks.

Single-Phase Transport Properties

Comparison of network-predicted absolute permeabilities and formation factors with the grid-predicted values are given in Table 3 and 4 respectively. There is a consistent trend in the network-predicted absolute permeabilities with GBA networks giving the highest

permeabilities while DOHT networks give the lowest permeabilities. Consequently, networks from DOHT skeletons have the highest network-predicted formation factors while networks from GBA skeletons have the lowest values. GBA network-predicted single-phase properties compares reasonably well with the grid-predicted values while those from DOHT are not in good agreement.

Table 3. Comparison of network-predicted with grid-predicted absolute permeabilities.

	Berea_01	**Berea_02**	**Bentheimer**	**Fontainebleau**
Grid results (mD)	1,345	409	1,949	2,551
GBA (mD)	1,213	327	2,228	2,688
PBTA (mD)	952	230	1,593	1,697
DOHT (mD)	666	141	1,012	1,180

Table 4. Comparison of network-predicted with grid-predicted formation factors.

	Berea_01	**Berea_02**	**Bentheimer**	**Fontainebleau**
Grid results	24,11	23,67	20,86	17,37
GBA	26.90	30.70	19.60	16.75
PBTA	29.75	33.60	23.40	22.50
DOHT	36.00	43.90	29.20	27.15

Multiphase Transport Properties

Primary Drainage and Waterflooding at Water-Wet Condition

The initial water saturation S_{wi}, established at the end of the primary drainage and the residual oil saturation S_{orw}, after waterflooding at water-wet conditions are summarised in Table 5. S_{wi} is mainly a function of clay content; and the different networks of each sample, give the same value of S_{wi} but slightly different values of S_{orw}. On a general note, networks from DOHT skeletons give largest S_{orw} while those from GBA skeletons give lowest values of S_{orw}.

Table 5. End-point saturations (S_{wi} and S_{orw}) for the different networks for each sample.

		Berea_01	**Berea_02**	**Bentheimer**	**Fontainebleau**
GBA	S_{wi}	0	0.10	0.03	0
	S_{orw}	0.34	0.38	0.35	0.31
PBTA	S_{wi}	0	0.10	0.03	0
	S_{orw}	0.35	0.39	0.37	0.33
DOHT	S_{wi}	0	0.10	0.03	0
	S_{orw}	0.38	0.40	0.40	0.35

Comparison of the primary drainage capillary pressure and relative permeability curves as well as imbibition relative permeability curves at water-wet conditions for the different networks of Berea_02, Bentheimer and Fontainebleau samples are shown in Figures 3 through 7. For each sample, the curves are similar and the slight differences in the capillary pressure curves are due to the differences in the throat radius distributions. The

results for Berea_01 sample show similar trend and is presented with other data in the section below.

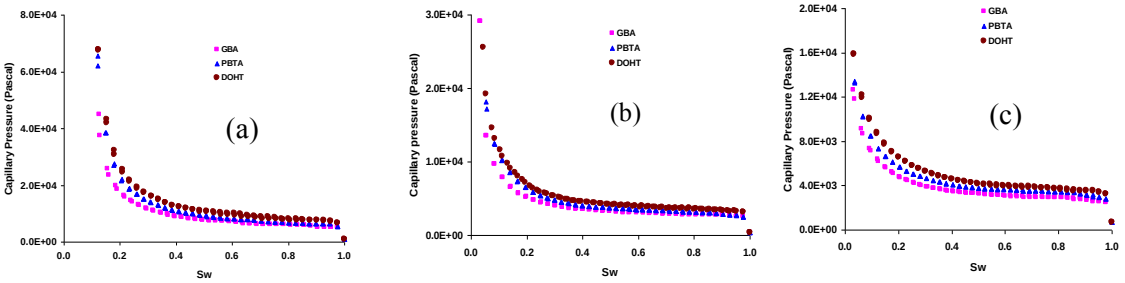

Figure 3: Comparison of primary drainage capillary pressure for (a) Berea_02, (b) Bentheimer and (c) Fontainebleau samples

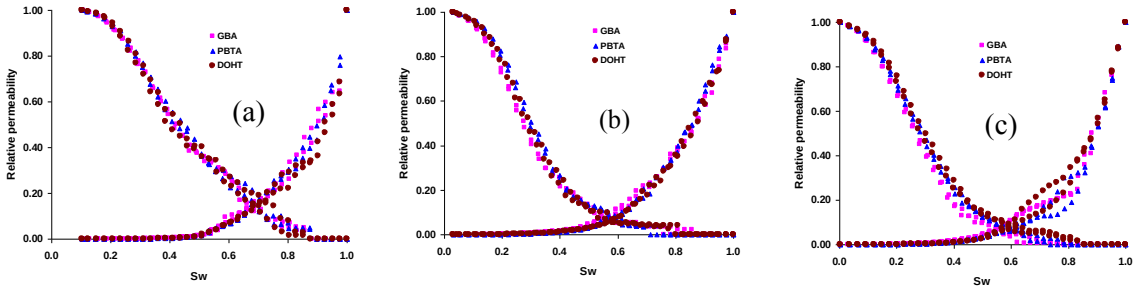

Figure 4: Comparison of primary drainage relative permeability curves (linear plot) for (a) Berea_02, (b) Bentheimer and (c) Fontainebleau samples

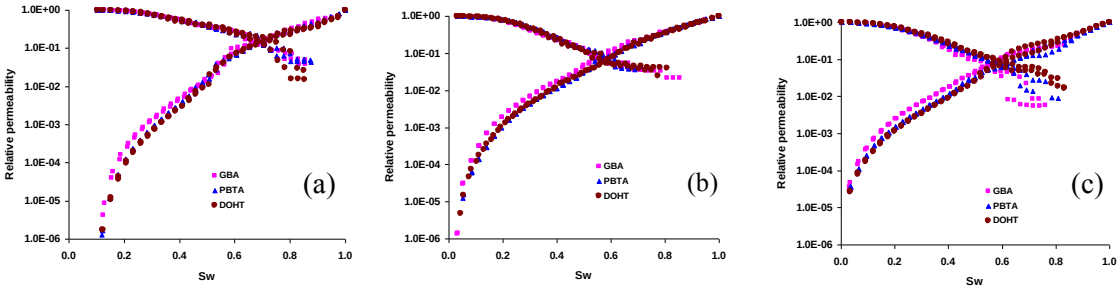

Figure 5: Comparison of primary drainage relative permeability curves (semi-log plot) for (a) Berea_02, (b) Bentheimer and (c) Fontainebleau samples

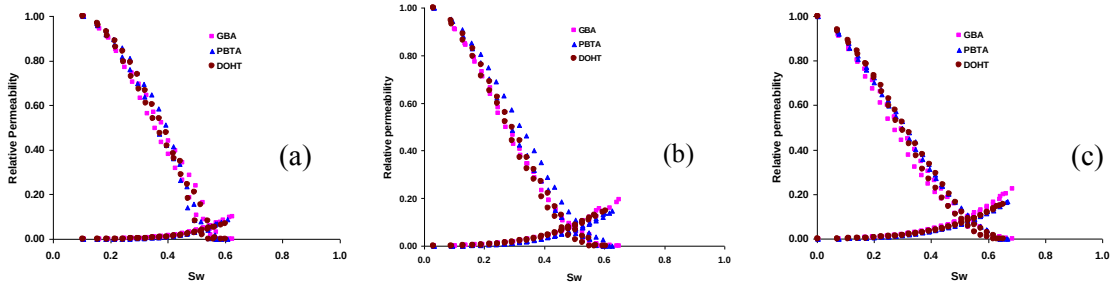

Figure 6: Comparison of imbibition relative permeability curves (linear plot) for (a) Berea_02, (b) Bentheimer and (c) Fontainebleau samples

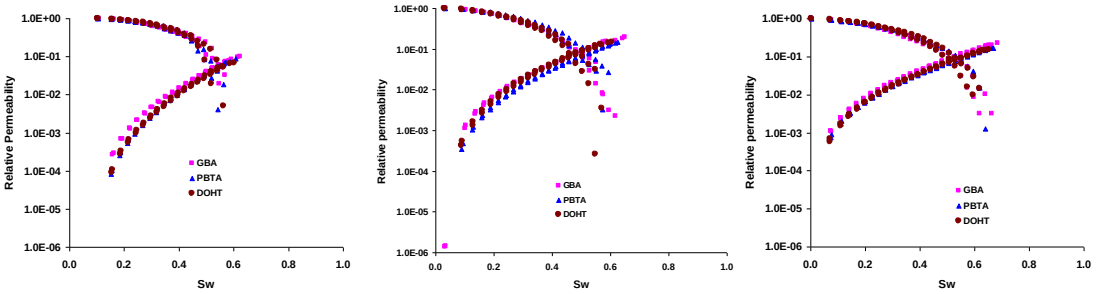

Figure 7: Comparison of imbibition relative permeability curves (semi-log plot) for (a) Berea_02, (b) Bentheimer and (c) Fontainebleau samples

Comparison of Simulated Results with Experimental Data

The predicted water-wet relative permeability curves for Berea_01, and Bentheimer samples are compared with published grid-predicted relative permeability data [1] and steady-state experimental data (Oak *et al.*, [10] and Øren *et al.*, [11]) in Figures 8 and 9. The grid-predicted data were obtained from (two-phase) steady-state LBM simulations at capillary numbers $Ca \approx 2.0\times10^{-6}$ [1].

The Berea sample used in the experiment had absolute permeability of 1,000 *mD* compared with grid-predicted permeabilities of 1,345 *mD*. For the Bentheimer samples however, three different samples with absolute permeabilities of 2,820 *mD*, 2,840 *mD* and 2,930 *mD* were used in the steady-state experiments compared with grid-predicted permeability of 1,949 *mD*.

While the reported and predicted S_{wi} (0.05 and 0.03 respectively) for the Bentheimer samples are similar, there are differences in S_{wi} (0.24 and 0 respectively) for Berea_01 sample. Hence, we normalise the experimental S_w to account for drainable pore volume for consistency when comparing experimental and predicted data. The difference in S_{wi} for Berea_01 is due to the absence of clay in the digitised image which is the main factor affecting irreducible water saturation in our models. The normalisation is done using:

$$S_w = \frac{S_w^* - S_{wi}}{1 - S_{wi}} \qquad (1)$$

where S_w^* is the total saturation of the wetting fluid.

The qualitative agreements between the different network-predicted relative permeability curves, experimental data and grid-predicted data are good for all the samples. However, the quantitative agreements vary from good to fair. The network-predicted results are obtained with contact angle distribution between 20^0 and 60^0 which is consistent with water-wet cases.

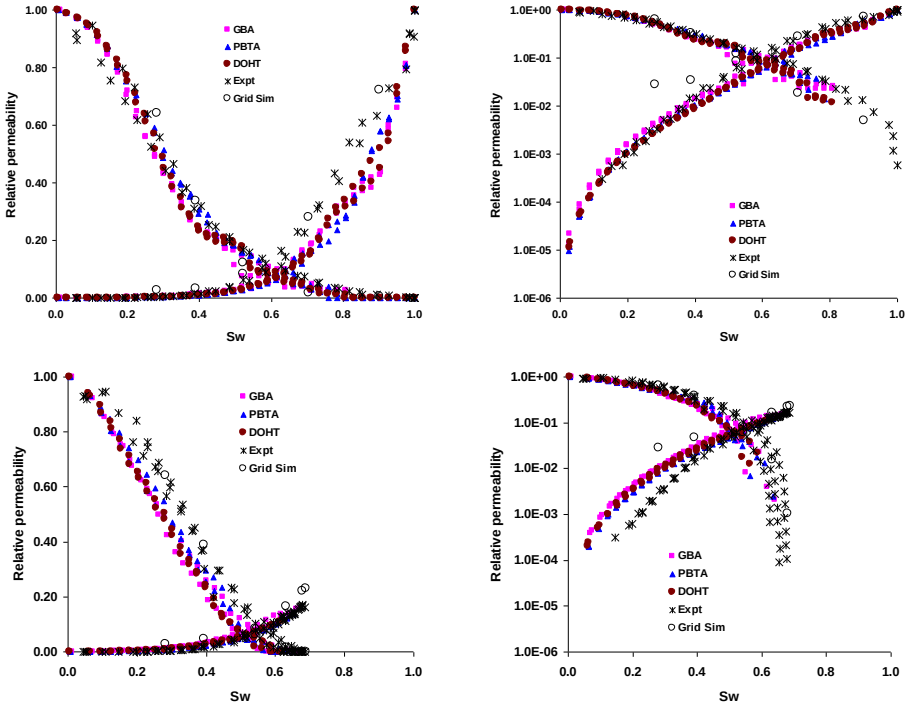

Figure 8: Comparison of network-predicted primary drainage (top) and imbibition (below) relative permeability curves with experimental data and grid-predicted data for Berea_01 sample at water-wet conditions.

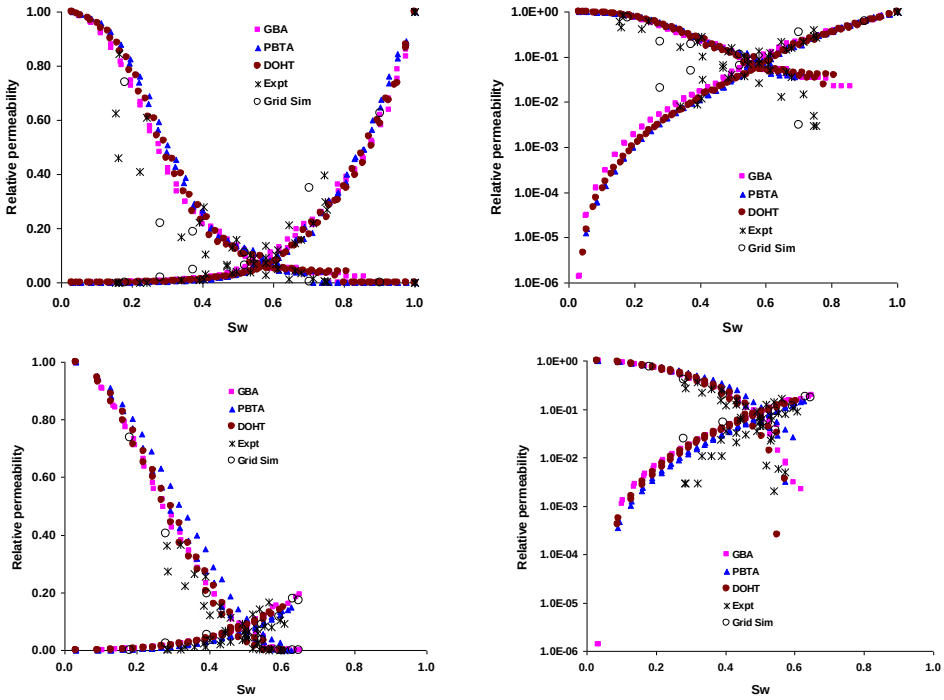

Figure 9: Comparison of network-predicted primary drainage (top) and imbibition (below) relative permeability curves with experimental data and grid-predicted data for Bentheimer sample at water-wet conditions.

Waterflooding at Mixed-Wet and Oil-Wet Conditions

In addition to the comparison with experimental data (water-wet conditions), we investigate the effect of wettability on the results obtained from the different networks. For this purpose, the wettability model used to perform the simulations at different wetting conditions is similar to the one described in details by Øren and Bakke [12]. For the mixed- and oil-wet case, we obtained Amott Water Indices I_w = 0.5 and 0 respectively. The relative permeability curves obtained from the different networks of Fontainebleau sample at mixed-wet (0.47, 0.46, and 0.49 for GBA, PBTA and DOHT respectively) and oil-wet (0.03, 0.04 and 0.03 for GBA, PBTA and DOHT respectively) conditions are very similar for the three different networks as depicted in Figures 10. We therefore conclude that for the entire range of wettability the three methods used to obtain the networks give similar results. Results for other samples show similar trends.

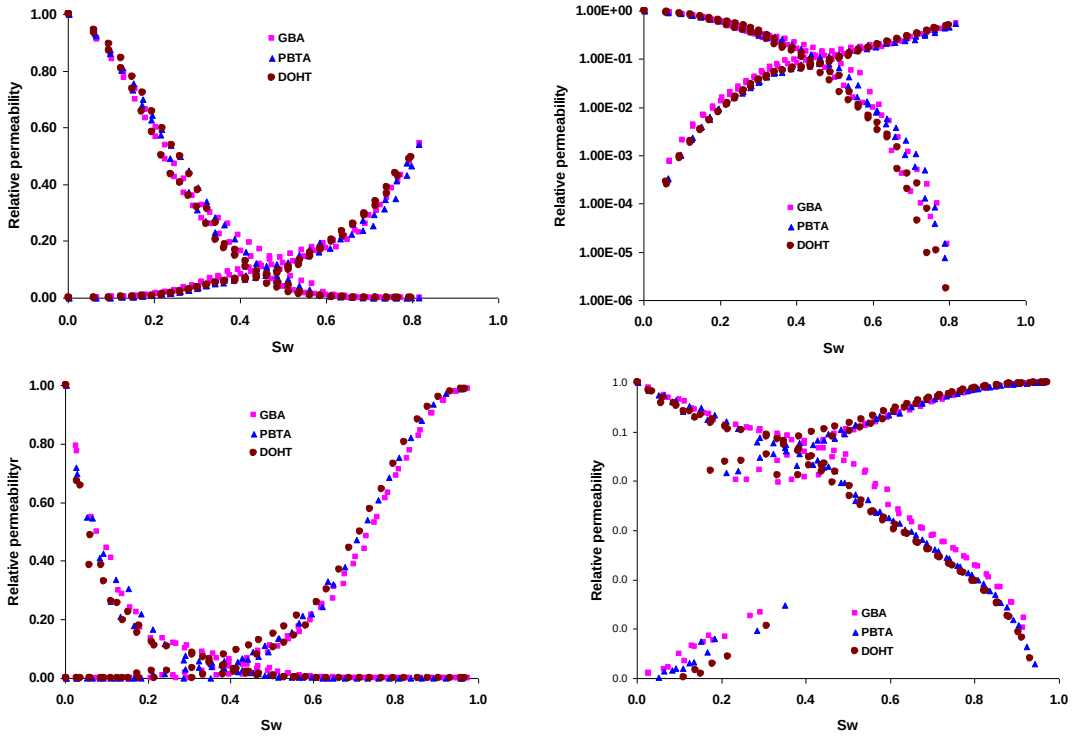

Figure 10: Comparison of relative permeability curves obtained from the different networks of Fontainebleau sample at mixed-wet (top) and oil-wet (below) conditions.

DISCUSSIONS OF RESULTS

Having presented all the results, we will attempt to provide some explanations to the differences observed in the network properties and single-phase transport properties, and also the consistency in the relative permeability curves. The main advantage of the medial axis skeletonization algorithm is that it preserves the topology of the pore space but identification and merging of pores are problematic. Hence, networks extracted from

PBTA and DOHT skeletons have higher number of (small) isolated and dead-end pores compared with those from GBA as shown in Table 6 and Figure 11 for Berea_02 sample.

Table 6. Comparison of the number of isolated and dead-end pores; and average aspect ratio for Berea_02

	Total number of pores	Number of isolated pores	Number of dead-end pores	Number of effective pores	Average aspect ratio
GBA	17,024	517	2123	14,384	2.80
PBTA	38,854	7,877	9,339	21,638	3.33
DOHT	37,615	8,654	8,554	20,407	3.71

Figure 11 shows the connectivity (coordination number) distribution for the three networks obtained from Berea_02 sample. The distribution for PBTA and DOHT are almost superimposed on each other while GBA network displays lower number of zero and one connected nodes. GBA network also shows slightly higher connectivity from coordination number of 2 upwards. Aside from these differences GBA network shows very similar behaviour as the two other networks and they are all similar topologically.

The average connectivities of the networks are calculated based on connected nodes only and higher average connectivities for all the GBA networks compared with others imply that they are much better connected with larger throat radius as shown in Figure 2. Consequently, GBA networks have much higher absolute permeability values and lower formation factors compared with others. Also, Table 6 shows that GBA networks have lower aspect ratio resulting in less snap-off events and therefore lower residual oil saturation, S_{orw} as shown in Table 5 at water-wet conditions compared with others.

The network-predicted absolute permeability and formation factor values from networks obtained from GBA compare reasonably well with the grid predicted data while predicted single-phase data from DOHT skeletons are not in good agreement quantitatively.

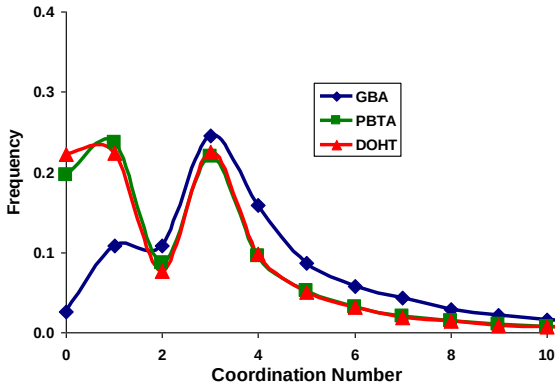

Figure 11: Connectivity distribution from the three different networks for the Berea_02 sample

The similarities / consistencies in the relative permeability curves from all networks for each sample at different wetting conditions are due to the fact that important features (topology / connectivity, e.t.c.) that are relevant to multiphase flow are well captured in the extracted skeletons and the networks are representatives. These also explain why there are good agreements between the network-predicted relative permeability curves, grid-predicted and experimental relative permeability data for both Berea and Bentheimer samples.

CONCLUSIONS

Using topologically equivalent skeletons extracted from three different skeletonization algorithms on four different samples, we generate different representative pore networks with the same geometrical and partitioning algorithm. Comparison of the network properties show, among other things, that the percentage difference in the number of pores ranges from 7% to 128%.

Multiphase displacements are simulated on the different pore networks and comparison of the absolute permeabilities and formation factors show differences in the absolute values but consistent trend for all the four samples. The differences in the absolute values are due to differences in the average connectivities and radius distributions of the different networks.

Despite the big differences in the pore-networks parameters, the primary drainage capillary pressure and relative permeability curves; initial water saturation; imbibition relative permeability curves at water-, mixed- and oil-wet conditions; and residual oil saturations after waterflooding at water-wet conditions for the different networks from each image are similar, consistent and within reasonable range.

We compare the network-predicted relative permeability curves from the different networks of Berea and Bentheimer with published grid-predicted relative permeability curves and available experimental data. The agreements between the different data are good.

Thus, we conclude that even though pore network extraction is a non-unique process, predicted multi-phase transport properties are consistent if the topology of the pore space is well preserved in the extracted skeleton. This study is currently being extended to assess the impact of the different skeletonization algorithms on three-phase relative permeability.

ACKNOWLEDGMENTS

The authors acknowledge Numerical Rocks AS for granting permission to publish this paper and this work is partly funded by Norwegian Research Council through PETROMAKS Project Number: 208772/E30, titled: “Physically based three-phase relative permeability relations”.

REFERENCES

1. Ramstad, T., N. Idowu, C. Nardi, and P.E. Øren, "Relative permeability calculations from two-phase flow simulations directly on digital images of porous rocks," *Transport in Porous Media*, (2011) doi: 10.1007/s11242-011-9877-8.
2. Lee, T.C., R.L. Kashyap, and C.N. Chu, "Building skeleton models via 3-D medial surface/axis thinning algorithms," *Computer Vision, Graphics, and Image Processing*, (1994), **56,** 6, 462–478.
3. Baldwin, C.A., A.J. Sederman, M.D. Mantle, P. Alexander, and L.F. Gladden, "Determination and characterization of the structure of a pore space from 3D volume images," *Journal of Colloid and Interface Science*, (1996) **181,** 79-92.
4. Liang, Z., M.A. Ioannidis, and I. Chatzis, "Geometric and topological analysis of three-dimensional porous media: pore space partitioning based on morphological skeletonization", *Journal of Colloid and Interface Science*, (2000) **221,** 13-24.
5. Lindquist, W.B., S.M. Lee, D. Coker, K. Jones, and P. Spanne, "Medial axis analysis of void structure in three-dimensional tomographic images of porous media," *Journal of Geophysical Research*, (1996) **101B,** 8297.
6. Bakke, S., and P.E. Øren, "3-D pore-scale modelling of sandstones and flow simulations in the pore networks," *SPE Journal*, (1997), **2**, 136-149.
7. Dong, H., S. Fjeldstad, L. Alberts, S. Roth, S. Bakke, and P.E Øren, " Pore network modelling on carbonate: a comparative study of different micro-CT network extraction methods" *Proceedings of the International Symposium of the Society of Core Analysts,* Abu Dhabi, UAE (2008).
8. Bhattad, P., C.S. Willson, and K.E. Thompson, "Effect of Network Structure on Characterization and Flow Modeling Using X-ray Micro-Tomography Images of Granular and Fibrous Porous Media," *Transport in Porous Media*, (2011), **90**, 363-391.
9. Ferreol, B. and D.H. Rothman, "Lattice-Boltzmann Simulations of Flow Through Fontainebleau Sandstone," *Transport in Porous Media*, (1995) **20,** 3-20.
10. Oak, M. J., L.E. Baker, and D.C. Thomas, "Three-Phase Relative Permeability of Berea Sandstone," *Journal of Petroleum Technology*, (1990), **42**, 1054-1061.
11. Øren, P.E., S. Bakke, and O.J. Arntzen, "Extending Predictive Capabilities to Network Models" SPE Journal, (1998), **3**, 324-336.
12. Øren, P.E., and S. Bakke, "Reconstruction of Berea Sandstone and Pore-Scale Modeling of Wettability Effects," *Journal of Petroleum Science and Engineering*, (2003), **39**, 177-199.